Performance Analysis of an Automated E-Pulse Target Discrimination Scheme

Jon E. Mooney, *Member, IEEE*, Zhi Ding, *Senior Member, IEEE*, and Lloyd S. Riggs, *Senior Member, IEEE*

***Abstract*—An automated E-pulse scheme for target discrimination was initially presented by Ilavarasan *et al.* in [1] without an analytic performance evaluation. Assuming that target responses are contaminated with white Gaussian noise, an automated E-pulse scheme is rigorously analyzed to yield a reliable measure of performance. The discrimination performance of this automated E-pulse scheme is determined quantitatively through the use of energy discrimination numbers (EDN's). Statistics of the EDN's are evaluated analytically to derive the probability of correct identification. The probability of identification as a function of signal-to-noise ratio (SNR) is evaluated using the theoretical scattering data for all potential targets to predict the performance of the automated E-pulse scheme. These theoretical results are corroborated by direct simulation of the discrimination scheme. In addition, the probability density functions of the EDN's are presented providing new physical insights into E-pulse performance as a function of target geometries and SNR.**

***Index Terms*—Pattern classification, radar target recognition.**

I. Introduction

THE concept of resonance based target discrimination has been studied by a number of researchers for many years. As evidenced by the many papers on the subject, the E-pulse and S-pulse techniques, which are closely related to Kennaugh's kill pulse [2], are popular and viable methods for performing resonance-based aspect-independent target discrimination. The E-pulse and S-pulse techniques, as described in the works by Rothwell *et al.* [3]–[5], provide a basis for target discrimination by selectively annihilating the resonant modes from the late-time transient response of a specific target. In these and subsequent works [6], [7], the discrimination performance of the E/S pulse methods were validated using theoretical as well as measured signature data. Recently, Ilavarasan *et al.* [1] quantitatively investigated the performance of an automated E/S pulse scheme under varying signal-to-noise ratio (SNR) conditions.

However, to date there has not been an accurate theoretical analysis of the performance of an automated E-pulse scheme. An accurate performance analysis allows one to evaluate the E-pulse discrimination scheme without having to resort to simulations. Furthermore, it allows one to better understand the fundamental principles of the E-pulse technique and it provides clearer insight into how performance improvements can be developed without having to undergo numerous simulation tests.

The approach taken in this investigation is to analyze the automated E-pulse scheme based on a standard probabilistic model. Based on the assumption that such an automated E-pulse scheme is designed to discriminate among a set of M targets whose signatory resonance modes are known, the objective of this paper is to develop an analytic performance measure in terms of the probability of identification. This measure is simply used to describe the probability of identifying any target belonging to the target library. In addition to the development of the probability of identification, numerical issues concerning the computation of this measure are addressed. Performance results, which are displayed for various levels of SNR, are given for different target library sizes. These performance results are verified by directly simulating the automated E-pulse scheme under varying SNR conditions.

II. E-Pulse Technique

The purpose of this section is to provide a brief overview of the E-pulse technique in order to establish notations and concepts, which will be used in the subsequent analysis. Although there are many published works on the E-pulse technique, the synopsis given here generally matches the discussions given by Ilavarasan *et al.* [1] and Rothwell *et al.* [5].

Based on the singularity expansion method (SEM) developed by Baum [8], [9], the late-time representation of the far-scattered field from a target due to a bandlimited transient excitation can be modeled as a sum of weighted exponentially damped sinusoids

$$r(t) = \sum_{n=1}^{N} a_n e^{\sigma_n t} \cos(\omega_n t + \phi_n) \quad t > T_l \tag{1}$$

where $s_n = \sigma_n + j\omega_n$ is the aspect independent natural frequency of the nth mode, and a_n and ϕ_n are the aspect-dependent amplitude and phase of the nth mode, respectively. The term T_l, which is also aspect dependent, denotes the beginning of the late-time period. The number of modes N in the response $r(t)$ depends on both the target and the frequency content of the excitation waveform.

As noted previously the E-pulse $f(t)$, which is a finite duration waveform, is constructed to annihilate the late-time response of a particular target or

$$f(t) * r(t) = 0, \qquad \text{for } t > T_L = T_l + T_e \tag{2}$$

where T_e denotes the duration of the E-pulse waveform. The Laplace transform of $f(t)$ is denoted as $F(s) \equiv \mathcal{L}\{f(t)\}$. In

Manuscript received February 19, 1999; revised November 18, 1999. The work of J. E. Mooney and Z. Ding was supported in part by the U.S. Army Research Office under Grants DAAH04-95-I-0200 and DAAH04-94-G-0252.

J. E. Mooney is with Raytheon Systems Company, Dallas, TX 75266 USA.

L. S. Riggs is with the Department of Electrical and Computer Engineering, Auburn University, Auburn, Alabama 36849 USA.

Z. Ding is with the Department of Electrical and Computer Engineering, University of Iowa, Iowa City, IA 53346 USA.

Publisher Item Identifier S 0018-926X(00)02459-5.

0018–926X/00$10.00 © 2000 IEEE

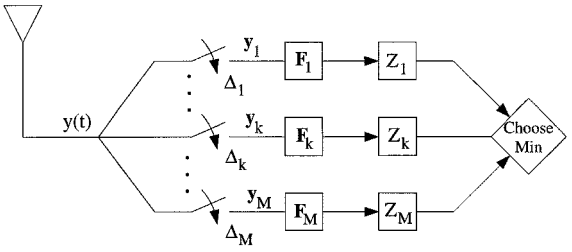

Fig. 1. The block diagram of an M-target E-pulse discrimination scheme.

order for the convolution in (2) to be zero, the following condition must be met:

$$F(s_n) = F(s_n^*) = 0, \qquad \text{for } n = 1, 2, \cdots, N \tag{3}$$

where the s_n are the natural frequencies of the target excited by the incident waveform.

If the natural frequencies of a target are known *a priori*, then an E-pulse waveform can be synthesized by representing $f(t)$ as a sum of subsectional basis functions

$$f(t) = \sum_{i=1}^{K} \alpha_n g(t - (i-1)\Delta) \tag{4}$$

where $g(t)$ represents the subsectional basis function of width Δ. Laplace transforming the expansion while enforcing the criterion given in (3) leads to a matrix equation for the amplitudes α_i. Letting $K = 2N$ results in a homogeneous matrix equation which has solutions for certain values of Δ. Solutions of the matrix equation exist for values of Δ given by

$$\Delta = \frac{p\pi}{\omega_n} \quad 1 \le n \le N, \quad p = 1, 2, \cdots. \tag{5}$$

To quantify the performance of the E-pulse technique for automation, the energy discrimination number (EDN) was developed [6]. The purpose of the EDN is to measure how much of the filtered signal $c(t) = f(t) * r(t)$ is present after normalizing by the energy of the E-pulse filter response

$$Z = \left[\int_{T_L}^{T_L+W} c^2(t)\,dt\right]\left[\int_0^{T_e} f^2(t)\,dt\right]^{-1}. \tag{6}$$

The target that yields the smallest EDN is then chosen as the correct target. Ideally, the energy discrimination number is zero provided the E-pulse is matched to the target producing the return. However, noise inevitably corrupts the return and prevents Z from vanishing completely. The choice of the time window W used in the computation of Z is somewhat arbitrary, but should at most be limited by the duration of the return.

III. Analytical Model

As a preface to our analysis, consider the block diagram shown in Fig. 1. The block diagram illustrates an automated E-pulse scheme designed to discriminate among a set of M targets. The diagram consists of M parallel signal paths which are fed by the receiving antenna. The kth path contains a

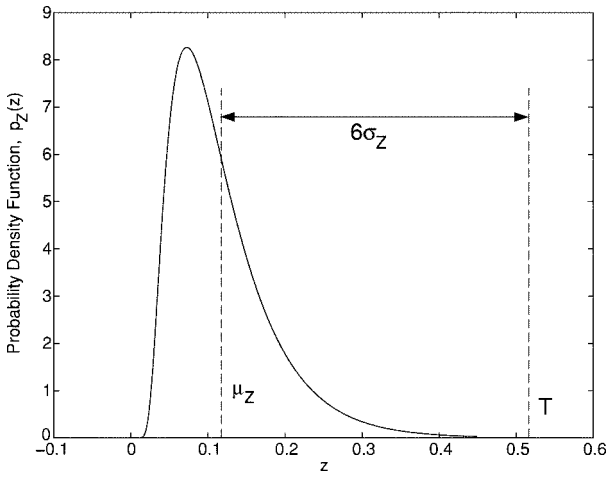

Fig. 2. An example of the pdf of the EDN.

sampler followed by an E-pulse filter F_k designed to annihilate the late-time response of the kth target. At the output of F_k, an energy discrimination number Z_k is computed and the path having the smallest Z_k is chosen as the correct target. For the purpose of mathematical tractability, the sample period of the kth sampler corresponds to the width Δ_k of the subsectional basis function used to construct F_k. In this fashion, the convolution operation in (2) can be represented as matrix-vector product (discrete convolution). Because of the presence of the M samplers, it is understood that the configuration shown in Fig. 1 is not necessarily a practical implementation of an automated E-pulse discrimination scheme. In previous works on the E-pulse technique, the measured responses were all sampled at a uniform rate, and the convolution was carried out as discussed in [10]. This approach avoids the use of M different samplers, but the convolution operation is inherently more complicated than the discrete convolution approach used here.

Assuming that a target exists and it belongs to the set of M possible candidates, the late-time portion of the received signal from the mth target can be expressed as

$$y(t) = r_m(t) + n(t) \quad t > T_l, \quad 1 \le m \le M \tag{7}$$

where $n(t)$ is zero mean white Gaussian noise with variance σ^2. The Gaussian noise assumption is justified for two reasons. First, it creates a mathematically tractable problem. Often, a suboptimal model for the randomness in the noise is used in order to obtain a final solution. Second, in an environment where a large number of noise sources exist, the central limit theorem dictates that the joint probability density of the noise will be Gaussian [11]. Furthermore, the white noise assumption is normally valid unless there is strong evidence that the noise is highly correlated.

The sampled version of $y(t)$ at a rate Δ_k is denoted by the vector $\mathbf{y}_k$ and (7) becomes

$$\mathbf{y}_k = \mathbf{r}_{mk} + \mathbf{n} \quad 1 \le m \le M, \quad 1 \le k \le M \tag{8}$$

where $\mathbf{r}_{mk}$ is the sampled vector of $r_m(t)$ at the rate Δ_k, and $\mathbf{n}$ is a normal random vector with zero mean and variance $\sigma^2\mathbf{I}$ ($\mathbf{I}$

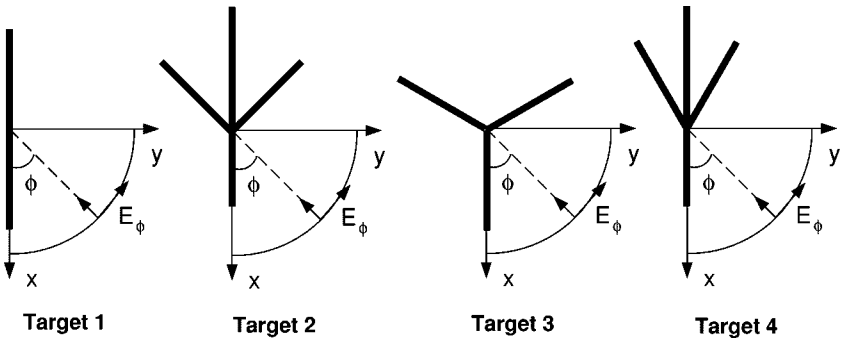

Fig. 3. Illustration of the four targets used in the analysis.

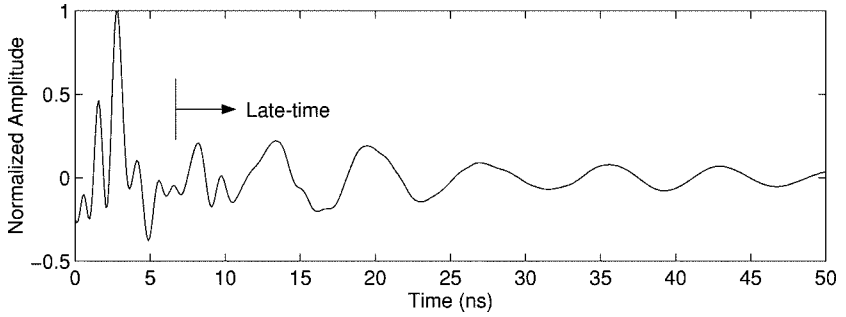

Fig. 4. The $\phi = 75^\circ$ backscattered response from the 45° swept-wing aircraft.

denotes the identity matrix). Furthermore, if we assume $\mathbf{y}_k$ contains Q_k samples, then the E-pulse filter $\mathbf{F}_k$ can be represented in matrix form as

$$\mathbf{F}_k \equiv \begin{bmatrix} \alpha_1 & 0 & 0 & \cdots & 0 \\ \vdots & \alpha_1 & 0 & \cdots & 0 \\ \alpha_{2N_k} & \vdots & \ddots & & \vdots \\ 0 & \alpha_{2N_k} & & \ddots & 0 \\ \vdots & 0 & \ddots & & \alpha_1 \\ \vdots & \vdots & & \ddots & \vdots \\ 0 & 0 & \cdots & \cdots & \alpha_{2N_k} \end{bmatrix}_{(2N_k+Q_k-1\times Q_k)}. \tag{9}$$

Recall that N_k represents the number of natural resonant modes that $\mathbf{F}_k$ is designed to extinguish. The energy discrimination number Z_k can be computed in terms of $\mathbf{y}_k$ and $\mathbf{F}_k$ as

$$Z_k = \mathbf{y}_k^H \mathbf{G}_k^H \mathbf{G}_k \mathbf{y}_k \tag{10}$$

where $\mathbf{G}_k$ is a submatrix of $\mathbf{F}_k$ containing the time window $T_L < t < T_L + W$ or

$$\mathbf{G}_k = \frac{\mathbf{F}_k(n_s : n_f, 1 : Q_k)}{||\mathbf{f}_k||} \tag{11}$$

where $\mathbf{F}_k(i : j, p : q)$ denotes extracting rows i through j and columns p through q, and $\mathbf{f}_k$ is a vector containing the amplitudes of the subsectional basis functions of the kth E-pulse filter. The indexes n_s and n_f denoting the beginning and ending of the time window are given by

$$n_s = \lceil (T_L/\Delta_k) \rceil + 1 \tag{12}$$

$$n_f = \lceil ((T_L + W)/\Delta_k) \rceil + 1 \tag{13}$$

and $\lceil x \rceil$ denotes the smallest integer above x. To compute (12) and (13) the beginning of the late-time period T_l must be determined. As shown by Ilavarasan *et al.* [1], the beginning of late time for backscattered responses is given by

$$T_l = T_b + T_p + 2T_{\text{tr}} \tag{14}$$

where T_{tr} is the maximum transit time of the target, T_p is the effective pulse duration used in the system, and T_b is an estimate of the time when the incident wave strikes the leading edge of the target. The time T_b is estimated from a threshold voltage V_T, which needs to be large enough to detect small signals, but small enough to maintain a small false alarm rate.

Because the response $\mathbf{y}_k$ is random, the EDN is a random variable. Furthermore, since the noise is assumed to be white and Gaussian, the EDN in (10) represents a sum of independent, squared Gaussian random variables. In addition, if we assume that the M sample rates in Fig. 1 do not commensurate, then it also follows from the white noise assumption that the Z_k for each signal path are independent. The assumption that the Δ_k do not commensurate is valid since it is not likely that the ω_n in (5) for all M targets are the same or are related by a rational number. As will be seen in the following section, the fact that the Z_k are

TABLE I
THE NATURAL FREQUENCIES OF THE FOUR TARGETS USED IN THE ANALYSIS

$\frac{s_n}{c}$	Thin Cylinder		45° Swept Wing		Perturbed Tripole		60° Swept Wing	
n	Real	Imag.	Real	Imag.	Real	Imag.	Real	Imag.
1	-0.2574	± 2.8743	-0.1142	± 2.6857	-0.2123	± 2.8645	-0.1320	± 2.7726
2	-0.3792	± 5.9329	-0.1748	± 3.0526	-0.2205	± 2.9538	-0.1149	± 3.2110
3	-0.4660	± 9.0117	-0.3215	± 3.6096	-0.2689	± 6.2325	-0.2992	± 3.5114
4	-0.5353	± 12.0955	-0.4772	± 6.6065	-0.5025	± 9.2240	-0.6288	± 6.5274
5	-0.5935	± 15.1775	-0.4059	± 7.9230	-0.4821	± 8.9461	-0.3005	± 7.9773
6	-0.6436	± 18.2533	-0.6182	± 9.3581	-0.4637	± 12.5192	-0.6102	± 9.3557
7	-0.6870	± 21.3193	-0.5594	± 11.0463	-0.7218	± 15.0031	-0.5647	± 11.0262
8	-0.7244	± 24.3726	-0.5560	± 12.0588	-0.7552	± 15.4586	-0.4928	± 12.0233
9	******	******	-0.5882	± 14.8595	-0.7043	± 18.6706	-0.7045	± 14.6847
10	******	******	-0.8985	± 15.4281	-0.9387	± 20.9337	-0.6975	± 15.6535
11	******	******	-0.6356	± 16.4076	-0.9835	± 21.5461	-0.4349	± 16.5412
12	******	******	-0.7755	± 18.7524	-0.9383	± 24.5863	-0.8272	± 18.6455
13	******	******	-0.6201	± 21.1990	******	******	-0.6110	± 21.2738
14	******	******	-0.9542	± 21.5145	******	******	-0.9544	± 21.7441
15	******	******	-0.7550	± 22.3478	******	******	-0.6915	± 22.1412

independent is crucial to developing a tractable expression for the probability of identification.

IV. PROBABILITY OF IDENTIFICATION

Assuming that the kth target is present, the probability of identifying the kth target is simply the probability the kth EDN Z_k is smaller than all the others, or

$$\begin{aligned} P_{I\,|\,k} &= P\,(\text{identifying } k\text{th target } |\, k\text{th target present}) \\ &= P(Z_1 > Z_k, \cdots, Z_{k-1} > Z_k, Z_{k+1} > Z_k, \cdots \\ &\quad Z_M > Z_k \,|\, k\text{th target present}). \end{aligned} \tag{15}$$

Applying the theorem of total probability [11] to (15), the expression for $P_{I\,|\,k}$ becomes

$$\begin{aligned} P_{I\,|\,k} = \int_{-\infty}^{\infty} & P(Z_1 > x, \cdots, Z_{k-1} > x, Z_{k+1} > x, \cdots, \\ & Z_M > x \,|\, Z_k = x) p_{Z_k}(x)\, dx \end{aligned} \tag{16}$$

where the p_{Z_k} denotes the probability density function (pdf) of Z_k. To conserve notation, the condition that the kth target is present has been implied in (16).

In general, evaluating (16) would be difficult because of the joint probability term. However, because the Z_k are independent under the assumption of incommensurate sampling rates and white Gaussian system noise $n(t)$, the joint conditional density in (16) can be simplified into products of individual conditional densities

$$\begin{aligned} P_{I\,|\,k} = \int_{-\infty}^{\infty} & P(Z_1 > x) \cdots P(Z_{k-1} > x) P(Z_{k+1} > x) \\ & \cdots P(Z_M > x)\, p_{Z_k}(x)\, dx \end{aligned} \tag{17}$$

from which follows:

$$\begin{aligned} P_{I\,|\,k} = \int_{-\infty}^{\infty} \Bigg[& \int_{x}^{\infty} p_{Z_1\,|\,k}(z_1)\, dz_1 \cdots \\ & \int_{x}^{\infty} p_{Z_{k-1}\,|\,k}(z_{k-1}) dz_{k-1} \int_{x}^{\infty} p_{Z_{k+1}\,|\,k}(z_{k+1}) dz_{k+1} \\ & \cdots \int_{x}^{\infty} p_{Z_M\,|\,k}(z_M)\, dz_M \Bigg] p_{Z_k}(x)\, dx \end{aligned} \tag{18}$$

TABLE II
RELEVANT DATA FOR THE E-PULSE DISCRIMINATION SCHEME SHOWN IN FIG. 1

kth Signal Path	Sampling Period Δ_k	F_k Matched To
1	0.1289/c	Dipole
2	0.1406/c	45° Swept Wing
3	0.1278/c	Perturbed Tripole
4	0.1419/c	60° Swept Wing

where $p_{Z_i\,|\,k}(z)$ is the pdf of Z_i given the kth target response. Recall that the expression in (18) is only the probability of identifying the kth target assuming the kth target is present. By obtaining a similar expression for the other $M-1$ targets, we obtain a measure of the discrimination capability of the E-pulse scheme or, equivalently, an average probability of identification

$$\text{Average } P_I = \sum_{m=1}^{M} P_{I\,|\,m} P_m \tag{19}$$

where P_m denotes the probability of the mth target being present. For our analysis, we will assume all M targets are equally likely to be present or $P_m = 1/M$.

V. COMPUTING THE PROBABILITY DENSITY FUNCTION

In order to evaluate (18) and, consequently, (19), the pdf $p_{Z_i\,|\,k}(z)$ must be computed. The derivation of the pdf is identical for all i and k. Hence, to conserve notation, the subscripts i and k on the variables in the following analysis are dropped.

As noted earlier, the quadratic form of the random variable Z in (10) essentially represents a weighted sum of squared Gaussian random variables. Performing an eigen-decomposition on the matrix $\mathbf{G}^H\mathbf{G}$, one obtains

$$\begin{aligned} Z &= \mathbf{y}^H \mathbf{V} \mathbf{\Lambda} \mathbf{V}^H \mathbf{y} \\ &= \mathbf{w}^H \mathbf{\Lambda} \mathbf{w} \end{aligned} \tag{20}$$

where $\mathbf{\Lambda}$ denotes the eigenvalues of $\mathbf{G}^H\mathbf{G}$ and is of the form

$$\mathbf{\Lambda} = \operatorname{diag}(\lambda_1, \cdots, \lambda_L, 0, \cdots, 0) \tag{21}$$

and $\mathbf{V}$ contains the associated (generalized) eigenvectors. Note that $\mathbf{V}$ is unitary. Since $\mathbf{y}$ is a Gaussian random vector, the linear transformation $\mathbf{w} = \mathbf{V}^H\mathbf{y}$ produces a Gaussian random vector with mean $\mu_{\mathbf{w}} = \mathbf{V}^H\mathbf{r}$ and variance $\sigma^2\mathbf{I}$. Expanding (20), the expression for Z becomes

$$Z = \sum_{l=1}^{L} \lambda_l w_l^2 \tag{22}$$

where w_l is the lth element of $\mathbf{w}$. The expansion in (22) represents a weighted sum of squared Gaussian, nonzero mean random variables. If the $\{\lambda_l\}$ were all unity, which would require $\mathbf{G}^H\mathbf{G}$ to be idempotent, then Z would have a noncentral χ^2 distribution [11]. Since $\mathbf{G}^H\mathbf{G}$ is generally not idempotent, we have to compute the pdf numerically.

The most efficient way to acquire the pdf of Z is through the use of characteristic functions. The characteristic function of the random variable β_l is defined as

$$\Phi_{\beta_l}(j\omega) = \int_{-\infty}^{\infty} e^{j\omega x} p_{\beta_l}(x)\, dx \tag{23}$$

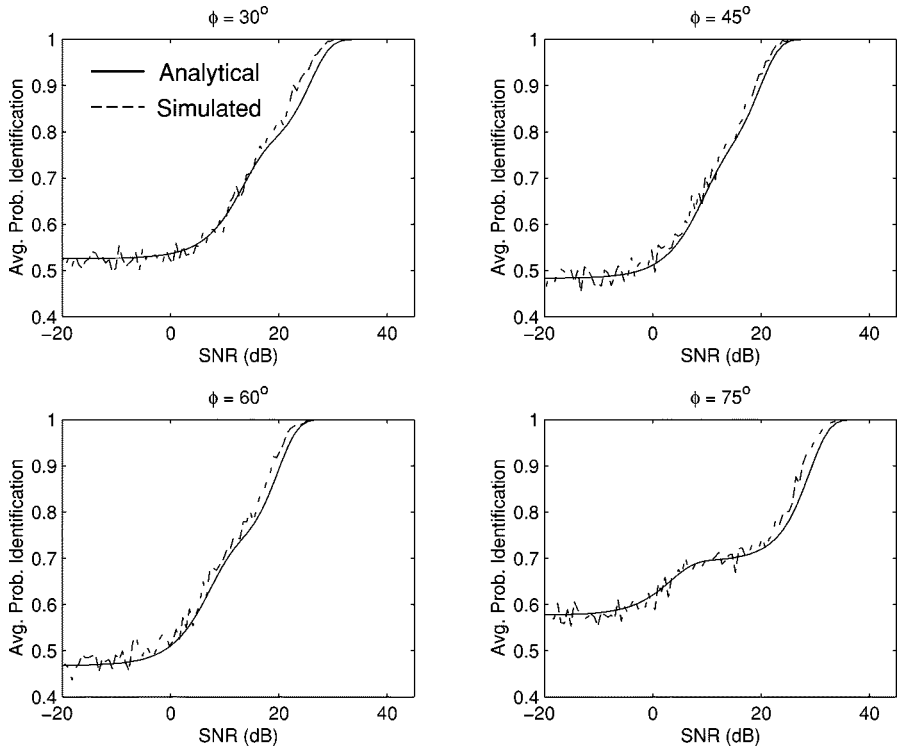

Fig. 5. Analytical and simulated results as a function of SNR for different aspect angles using targets 1 and 2.

which represents the Fourier transform of the pdf $p_{\beta_l}(x)$. By letting $\beta_l = \lambda_l w_l^2$ in (22), the characteristic function of Z can be computed as

$$\Phi_Z(j\omega) = \prod_{l=1}^{L} \Phi_{\beta_l}(j\omega) \tag{24}$$

since the β_l are independent random variables [11]. Furthermore, the form of the characteristic function of β_l is well known [12] and is given by

$$\Phi_{\beta_l}(j\omega) = \frac{\lambda_l}{|\lambda_l|(1 - j\omega 2\lambda_l\sigma^2)^{1/2}} \exp\left[\frac{j\omega\mu_{w_l}^2\lambda_l}{1 - j\omega 2\lambda_l\sigma^2}\right] \tag{25}$$

where μ_{w_l} is the lth element of the mean vector $\mu_{\mathbf{w}}$. To obtain $p_Z(z)$, we use the inverse Fourier transform

$$f_Z(z) = \frac{1}{2\pi}\int_{-\infty}^{\infty} \Phi_Z(j\omega)e^{-j\omega z}d\omega. \tag{26}$$

An illustration of a typical density function $p_Z(z)$ for the EDN is shown in Fig. 2. The initial step in computing $p_Z(z)$ numerically begins with computing the characteristic function $\Phi_{\beta_l}(j\omega)$. In order to compute $\Phi_{\beta_l}(j\omega)$ numerically, a sample frequency ω_s must be chosen judiciously. As can be seen from Fig. 2, $p_Z(z)$ is essentially band limited. Thus, following the Nyquist sampling theorem, an appropriate choice for ω_s is

$$\omega_s = \frac{\pi}{T} \tag{27}$$

where T denotes some point on the tail end of $p_Z(z)$. From the mean μ_Z and variance σ_Z^2 of Z, it is possible to develop an expression for T that will prevent aliasing. As shown in Fig. 2, a judicious choice for T is given by

$$T = \mu_Z + 6\sigma_z. \tag{28}$$

Since the mean and variance of $\mathbf{w}$ are known, μ_z and σ_Z^2 follow from (22) and are expressed as

$$\mu_Z = \sum_{l=1}^{L} \lambda_l\left(\sigma^2 + \mu_{w_l}^2\right) \tag{29}$$

$$\sigma_Z^2 = \sum_{l=1}^{L} \lambda_l^2\left(3\sigma^2 + 6\sigma^2\mu_{w_l}^2 + \mu_{w_l}^4\right) + 2\sum_{l=1}^{L-1}\left\{\sum_{p=l+1}^{L} \lambda_l\lambda_p\left[\sigma^4 + \sigma^2\left(\mu_{w_l}^2 + \mu_{w_p}^2\right) + \mu_{w_l}^2\mu_{w_p}^2\right]\right\} - \mu_Z^2. \tag{30}$$

The following steps summarize the computation of the pdf $p_{Z_i\,|\,k}(z)$.

- Specify the average noise power σ^2.
- Perform an eigen-decomposition of the matrix $\mathbf{G}^H\mathbf{G}$ for the ith E-pulse filter.
- Let $\mathbf{r}$ be the sampled response from the kth target.
- Compute the mean vector $\mu_w = \mathbf{V}^H\mathbf{r}$.
- Compute μ_Z and σ_Z^2 using (29) and (30), respectively.
- Compute the sample frequency ω_s using (27) and (28).
- Compute $\Phi_{\beta_l}(j\omega)$ using (25) for $l = 1, \cdots, L$.
- Multiply $\{\Phi_{\beta_l}(j\omega)\}$ to obtain $\Phi_Z(j\omega)$.
- Inverse Fourier transform $\Phi_Z(j\omega)$ to obtain $p_{Z_i\,|\,k}(z)$.

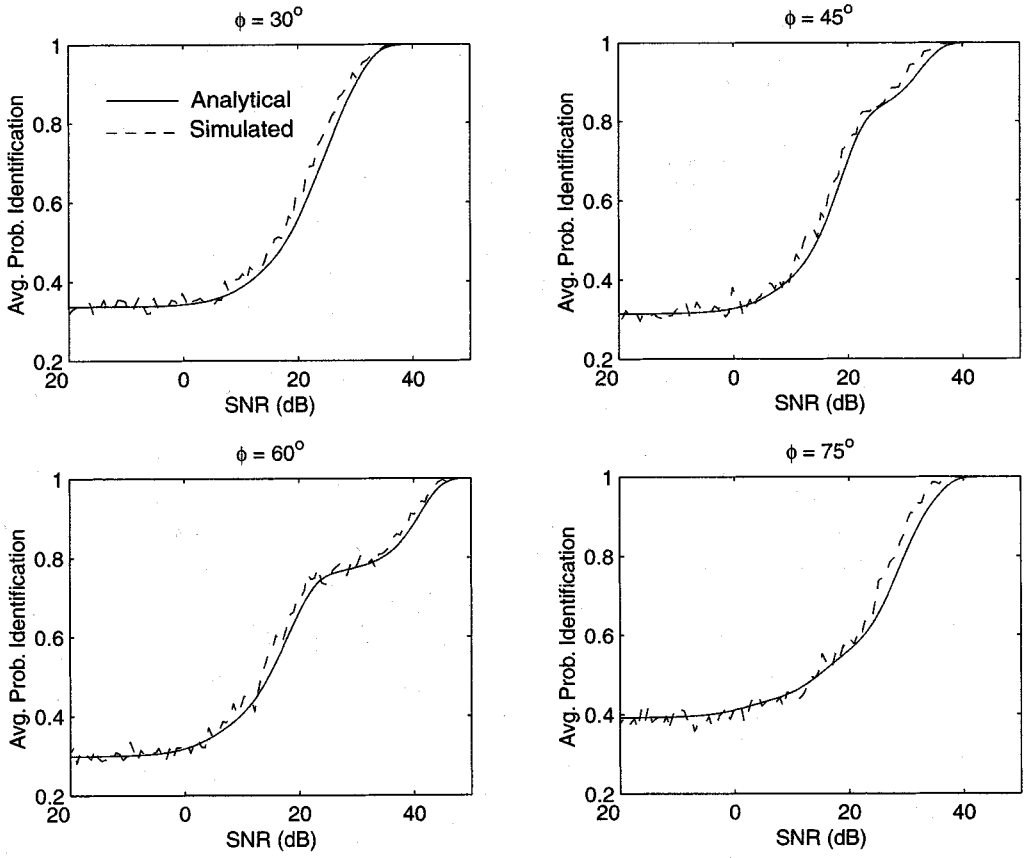

Fig. 6. Analytical and simulated results as a function of SNR for different aspect angles using targets 1, 2, and 3.

As noted earlier, before $P_{I\,|\,k}$ can be determined, the pdf's for the remaining $M-1$ EDN's must be obtained. Hence, the above process is repeated $M-1$ times.

VI. Analytical and Simulation Results on Specific Targets

In this section, we demonstrate the reliability of our analytical model. Results demonstrating the performance of the automated E-pulse discrimination scheme shown in Fig. 1 are provided. The performance results are represented by plotting the probability of identification as a function of SNR. Results are given for different target library sizes as well as varying aspect angles. The probability of identification is determined analytically using (18) and (19). To verify the analytical results, the probability of identification is determined directly through Monte Carlo simulation.

The targets used in developing the analytical and simulated results are shown in Fig. 3. Target 1 is a simple 1 meter long thin cylinder lying along the x axis and centered at the origin. Target 2 is a swept wing aircraft model. The fuselage of the aircraft lies along the x axis with forward and aft sections of $1/3$ m and $2/3$ m, respectively. The wings are swept back 45° from the normal to the fuselage and are $1/2$ m in length. Target 3 is a perturbed symmetric tripole. Two of its arms are have a length of $1/2$ m, and the third arm is 0.5238 m long. Target 4 is also a swept wing aircraft model similar to Target 2. The only distinguishing feature between the two is the angle at which the wings are swept back. The wings on target 4 are swept back 60° from the normal to the fuselage. As illustrated in Fig. 3, the aspect angle ϕ is defined to be in the plane of the target and is measured from the x axis. All of the targets discussed here are constructed with thin cylinders having radii of 0.005 m.

The scattering data used in the experiment are the theoretical impulse responses of the four targets mentioned above. These responses were obtained using the SEM, which was cast into numerical form via the method of moments [13]. The poles that were used in obtaining the backscattered field from each target are listed in Table I. Note that the poles have been normalized by the speed of light c. The first eight complex conjugate pole pairs were used in computing the backscattered field impulse response of the 1-m-thin cylinder. In order to ensure that the same bandwidth was used among each of the four targets, it was necessary to use the first 15 conjugate poles pairs to compute the impulse responses of the 45° and 60° swept wing aircraft models. Similarly, the first twelve poles of the perturbed symmetric tripole were used in computing its impulse response. Fig. 4 shows the backscattering response of the 45° (target 2) due to an impulsive plane wave incident from $\phi = 75°$. It should be noted here that the impulse responses for all targets were computed using a Class I coupling coefficient [14]; thus, the early time portion of the responses are inaccurate.

Based on the target data given, Table II presents all the relevant data for a four target E-pulse discrimination scheme as

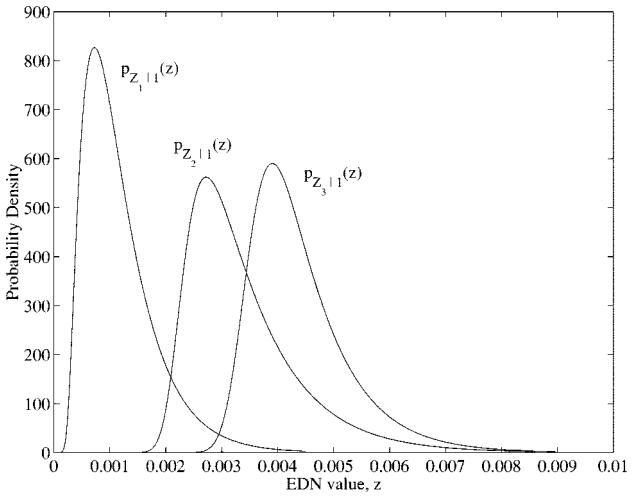

(a)

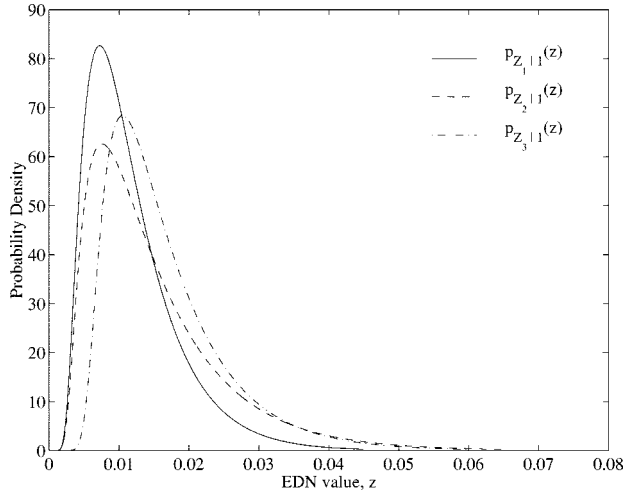

(b)

Fig. 7. The pdf's of the energy discrimination numbers for the three target case. The pdf's were computed using the scattering data for the thin cylinder at two different values of SNR. (a) $\mathrm{SNR} = 30$ dB. (b) $\mathrm{SNR} = 20$ dB.

illustrated in Fig. 1. As discussed in Section II, the kth signal path contains the E-pulse filter designed to annihilate the response from the kth target. For example, the second signal path contains the E-pulse filter matched to Target 2. The E-pulse filters for all targets in Fig. 3 are constructed using their respective resonances as listed in Table I. Furthermore, the sampling period for each target given in Table II is the smallest sampling period that can be calculated based on the resonance data given in Table I.

A. Analytical Results

The initial step in determining the probability of identification analytically for a specific SNR value is to evaluate $P_{I\,|\,k}$ for each of the M targets. Evaluating $P_{I\,|\,k}$ as shown in (18) requires us to assume that the kth target is present. Consequently, the pdf of each EDN must be computed using the signature data from the kth target. In order to compute each pdf for a specific SNR value, the average power of the noise-free return from the

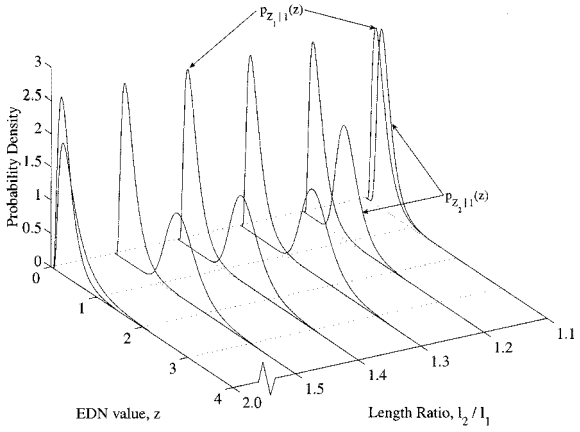

Fig. 8. A comparison of the EDN pdf's for varying length ratios of the thin cylinder. The pdf's were computed using the scattering data for the 1-m thin cylinder at an SNR of 10 dB.

kth target $r_k(t)$ must be determined. The average power of $r_k(t)$ is defined in the usual way as

$$P_k = \frac{1}{T}\int_0^T r_k^2(t)\,dt. \tag{31}$$

Knowing P_k, the average noise power σ^2 can be calculated for a specific SNR (in dB) as

$$\sigma^2 = P_k 10^{-\mathrm{SNR}/10}. \tag{32}$$

For the signature data used in these results, the end time T of the integration is arbitrarily chosen to be 50 ns.

Once σ^2 is known, the pdf of each EDN in $P_{I\,|\,k}$ is computed numerically as discussed in Section V. A critical step in computing the pdf is the eigen-decomposition of the matrix $\mathbf{G}^H\mathbf{G}$. Before this operation can be performed, the matrix $\mathbf{G}$, whose size is dependent on the size of the integration window as defined in (12) and (13) must be formed. Since we are using the theoretical impulse responses as the scattering data, the beginning of the late-time period T_l is taken to be twice the maximum transit time of the target. Furthermore, the integration window W for the EDN is arbitrarily chosen to be 15 ns. Following the eigen-decomposition operation, the characteristic functions used in obtaining each pdf are computed using 2048 equally spaced points. This choice of the number points allows the operation in (26) to be carried out using the fast Fourier transform (FFT).

B. Simulation Results

To verify the analytical results, the probability of identification is determined using a Monte Carlo simulation. The Monte Carlo simulation is essentially a direct implementation of the scheme illustrated in Fig. 1. In each simulation, a target from the target library is selected at random. The selection process is conditioned by the assumption that each target is equally likely to be present. Once a target has been selected, white Gaussian noise is added to the corresponding signature data of the target. The noise is scaled appropriately using (32) to yield a specific SNR.

After adding noise to the signature, the corrupted return is passed down each of the M signal paths as shown in Fig. 1. The

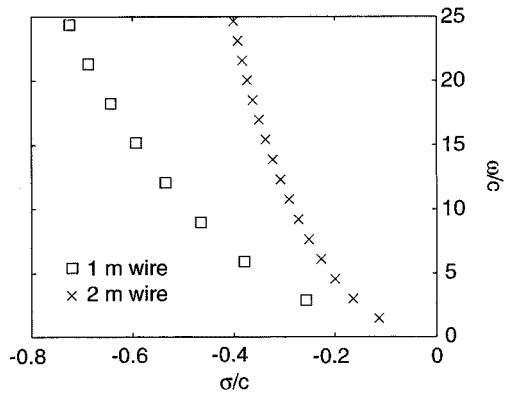

Fig. 9. Pole locations of the 1- and 2-m thin wires with radii of 0.005 m.

EDN in each signal path is computed using (10). As in the analytical results, the integration window W used in computing the EDN is arbitrarily chosen to be 15 ns. The path containing the minimum EDN is selected as the correct target. This process is repeated 1000 times at a specific value of SNR, and the number of correct identifications is tallied. The simulation is performed over a range of SNR values.

C. Results

Figs. 5, 6, and 11 show performance results for library sizes of two, three, and four targets, respectively. The results shown in Fig. 5 were obtained using only targets 1 and 2 as illustrated in Fig. 3. The analytical and simulated results, which were computed over an SNR range of -20 to 50 dB, agree remarkably well for all aspect angles considered. At low values of SNR, the probability of identification is approximately $1/2$, which means the performance in not any better than a random guess. This result is expected since we initially assumed that each target in the library has an equal probability of being present. As the SNR increases, the probability of identification gradually approaches unity. Depending on the aspect angle, the probability of identification reaches unity at approximately 30 dB.

Fig. 6 shows the performance results for a target library consisting of the thin cylinder, the 45° swept wing model, and the perturbed tripole. The agreement between the analytical and simulation results is very good for all aspect angles. The probability of identification is $1/3$ at -20 dB and eventually reaches unity at approximately 40 dB. To provide physical insight, the density functions of the EDN's for the three target scheme are shown in Fig. 7. The pdf's were computed using the scattering data from the thin cylinder (Target 1). Figs. 7(a) and (b) illustrate the pdf's assuming an SNR of 30 and 20 dB, respectively. A significant attribute of Fig. 7 is it provides the range and relative frequency of the energy discrimination numbers for a specific SNR when the thin cylinder is assumed present. As shown in Fig. 7(a), the pdf $p_{Z_1|1}(z)$, which corresponds to the correct target, is densest at a lower EDN value compared to the densest regions of Z_2 and Z_3. Hence, in this case, the thin cylinder will, on the average, be chosen as the correct target. When the SNR is decreased to 20 dB as in Fig. 7(b), the pdf's overlap and broaden in range. The overlapping characteristic of the pdf's is directly related to the performance of the discrimination scheme. By studying the distribution of the EDN's, the effects of aspect angle, observation window, and other target parameters on the performance of the discrimination scheme can be determined.

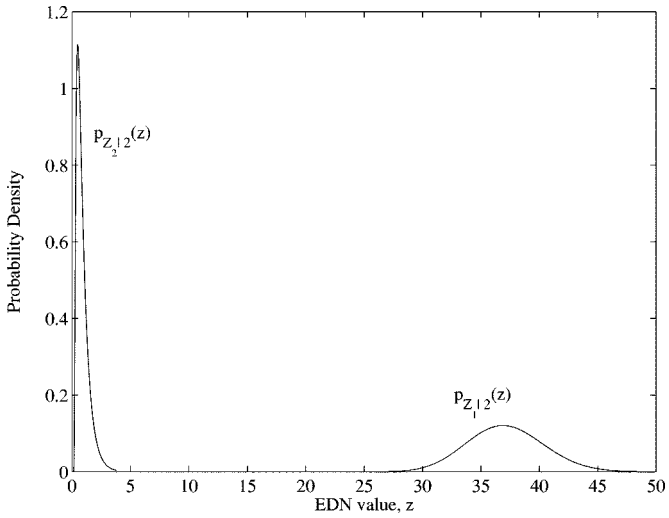

Fig. 10. The probability density functions of the energy discrimination numbers for the $l_2/l_1 = 2.0$ case. The pdf's were computed using the scattering data for the 2-m cylinder with an SNR of 10 dB.

To determine how the physical size of a target affects the performance of the E-pulse discrimination scheme, a parametric analysis of thin cylinders of varying lengths was performed. The thin cylinders used in the analysis have lengths of 1, 1.1, 1.2, 1.3, 1.4, 1.5, and 2 m and radii of 0.005 m. The natural frequencies of the thin cylinders were found numerically, and their corresponding E-pulse filters were constructed as outlined in Section II. The analysis consists of a two target discrimination scheme designed to distinguish the 1-m cylinder (Target 1) from one of the other longer cylinders (Target 2). The 1-m thin cylinder is assumed to present at an aspect angle of 75°, and the pdf's of the two EDN's (Z_1 and Z_2) are computed. This process is repeated for each of the other thin cylinders longer than 1 m. Fig.8 illustrates the results of this analysis for an SNR of 10 dB. The pdf $p_{Z_1|1}(z)$ corresponds to the EDN matched to the 1-m thin cylinder (the correct target) and the pdf $p_{Z_2|1}(z)$ corresponds to the EDN matched to one of the longer cylinders. The two pdf's are plotted according to the ratio of the lengths of the two cylinders. As mentioned earlier, the overlapping characteristic of the pdf's is indicative of the performance of the discrimination scheme. From Fig. 8, one observes that the performance of the discrimination scheme improves, as expected, with increasing length ratio. It is also interesting to note that once the length ratio exceeds a certain threshold, around 1.3, a greater increase does not result in a continued spreading of the EDN densities. In fact, beyond a length ratio of 1.3, the density functions actually converge and eventually overlap when the length ratio reaches 2.0.

The convergence of the pdfs $p_{Z_1|1}(z)$ and $p_{Z_2|1}(z)$ for the case $l_2/l_1 = 2.0$ can be explained by observing the pole locations of the 1 and 2-m thin wires as shown in Fig. 9. Observe that the oscillation frequency ω of the second-order pole of the 2-m wire is approximately the same as the oscillation frequency of the fundamental pole of the one meter wire. In fact, Fig. 9 reveals the relationship $\omega_{n,1} \approx \omega_{2n,2}$ where $\omega_{n,1}$ and $\omega_{n,2}$ denote

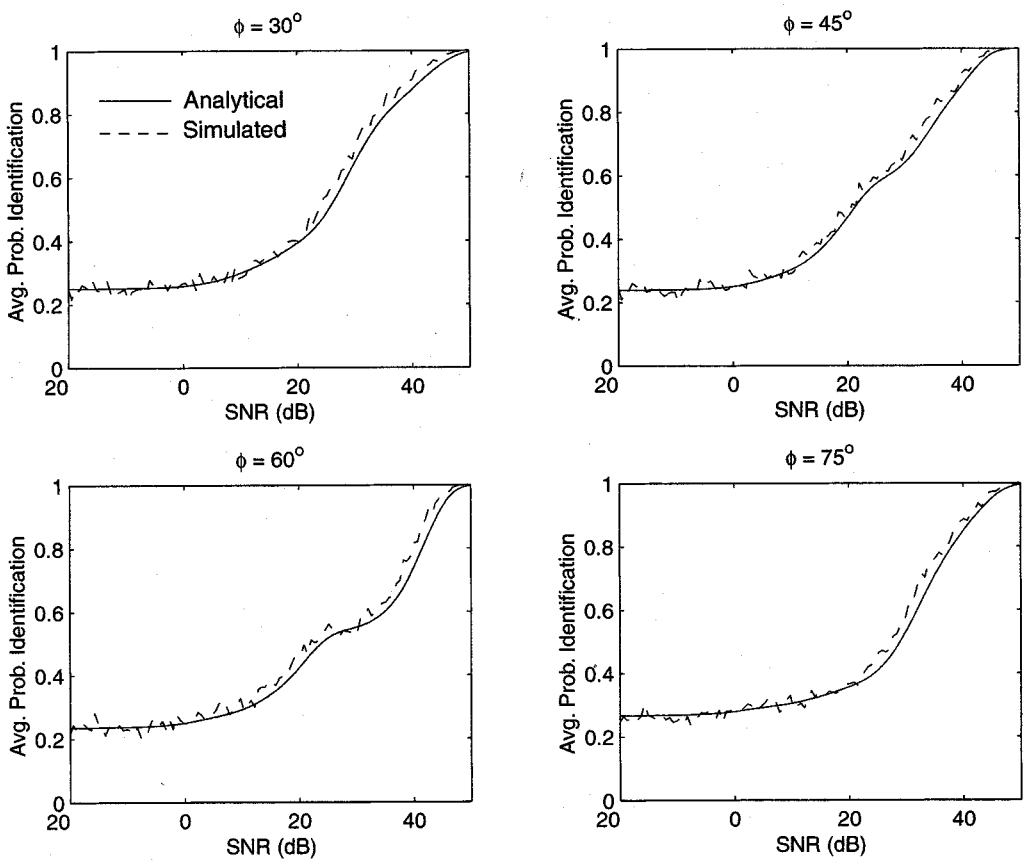

Fig. 11. Analytical and simulated results as a function of SNR for different aspect angles using targets 1, 2, 3, and 4.

the oscillation frequency of the nth order pole of the 1 and 2-m wire, respectively. Hence, when the response from the 1-m wire is passed through the E-pulse filter for the 2-m wire, the zero's designed to annihilate the resonances of the 2-m target also partially annihilate the resonances of the 1-m target. This does not suggest discrimination of these two targets is impossible. Indeed, for higher SNR levels, discrimination performance improves. However, for a given SNR, discrimination appears more difficult for integer length ratios than for noninteger length ratios when the smaller target is present.

Another interesting result of the $l_2/l_1 = 2.0$ case is produced when the 2-m wire target is assumed to be present. Unlike the previous situation, the response of the 2-m wire contains resonances where the E-pulse filter for the 1-m target $(\mathbf{F}_1)$ does not have zero's. In particular, the fundamental resonance, which typically couples the strongest, passes through $\mathbf{F}_1$ essentially unabated. As a result, a significant separation of the EDN densities $p_{Z_1|2}(z)$ and $p_{Z_2|2}(z)$ occurs even though the SNR is 10 dB. This result is shown in Fig. 10.

One can conclude from the above analysis that the functional dependence of the EDN's on different variables of the electromagnetic interaction problem can be separately considered resulting in an improved understanding of how the performance of the E-pulse discrimination scheme can vary with respect to these parameters. The ability to compute the probability densities of the EDN's effectively extends ones ability to understand and gain physical insights into how complex electromagnetic interactions ultimately affect different target discrimination schemes.

Finally, Fig. 11 presents the performance results for all the targets illustrated in Fig. 3. As in the two and three target cases, the agreement between the analytical and simulation results is excellent for all aspect angles. The probability of identification is $1/4$ at -20 dB and eventually reaches unity at approximately 48 dB. It should be noted here that the performance results presented in Figs. 5, 6, and 11 are dependent on the target geometries and the implementation of the automated E-pulse scheme. For example, the simulation results given in [15] demonstrate a better overall performance of the E-pulse scheme than do the results presented here. However, the results obtained in [15] were obtained using signature data that was sampled more densely than the signature data used in the results given in Figs. 6 and 11. Nonetheless, the theoretical analysis we have proposed can be applied equally to other targets and other forms of implementations.

VII. Conclusion

In this paper, the performance of an automated E-pulse scheme for target identification in white Gaussian noise was evaluated analytically. By evaluating the probability densities of the energy discrimination numbers, a theoretical method for

determining the probability of identifying a target from a family of M targets was developed. Results illustrating the probability of identification as a function of SNR were presented for different target library sizes and aspect angles. From these analytical results, it is clear that previous simulation results on the E-pulse method agree very well with our analysis and are reliable indications of the method's performance. To the best of our knowledge, the results given herein represent the first successful theoretical analysis of the performance of an automated E-pulse scheme.

The methodologies adopted here can be extended to the analysis of other target identification methods. In the future, the authors would like to perform a similar performance analysis of the E-pulse technique using measured late-time scattering data. Moreover, an approach similar to the one presented here will be used to evaluate the performance of another target discrimination scheme, which is based on a generalized likelihood ratio test [15].

REFERENCES

[1] P. Ilavarasan, J. E. Ross, E. J. Rothwell, K. M. Chen, and D. P. Nyquist, "Performance of an automated radar target discrimination scheme using E pulses and S pulses," *IEEE Trans. Antennas Propagat.*, vol. 41, pp. 582–588, May 1993.

[2] E. M. Kennaugh, "The K-pulse concept," *IEEE Trans. Antennas Propagat.*, vol. AP-35, pp. 327–331, Mar. 1981.

[3] E. Rothwell, D. P. Nyquist, K. M. Chen, and B. Drachman, "Radar target discrimination using the extinction-pulse technique," *IEEE Trans. Antennas Propagat.*, vol. AP-33, pp. 929–937, Sept. 1985.

[4] K. M. Chen, D. P. Nyquist, E. J. Rothwell, L. L. Webb, and B. Drachman, "Radar target discrimination by convolution of radar return with extinction-pulses and single-mode extraction signals," *IEEE Trans. Antennas Propagat.*, vol. AP-34, pp. 896–904, July 1986.

[5] E. J. Rothwell, K. M. Chen, D. P. Nyquist, and W. Sun, "Frequency domain E-pulse synthesis and target discrimination," *IEEE Trans. Antennas Propagat.*, vol. AP-35, pp. 426–434, Apr. 1987.

[6] C. E. Baum, E. J. Rothwell, K. M. Chen, and D. P. Nyquist, "The singularity expansion method and its application to target identification," *Proc. IEEE*, vol. 79, pp. 1481–1492, Oct. 1991.

[7] K. M. Chen, D. P. Nyquist, E. J. Rothwell, and W. M. Sun, "New progress on E/S pulse techniques for noncooperative target recognition," *IEEE Trans. Antennas Propagat.*, vol. 40, pp. 829–833, July 1992.

[8] C. E. Baum, "On the singularity expansion method for the solution of electromagnetic interaction problems," Kirtland AFB, Air Force Weapons Lab., Albuquerque, NM, Interaction Note 88, 1971.

[9] C. E. Baum, "SEM backscattering," Kirtland AFB, Air Force Weapons Lab., Albuquerque, NM, Interaction Note 476, 1989.

[10] E. J. Rothwell, K. M. Chen, and D. P. Nyquist, "Extraction of the natural frequencies of a radar target from a measured response using E-pulse techniques," *IEEE Trans. Antennas Propagat.*, vol. AP-35, pp. 715–720, June 1987.

[11] A. Papoulis, *Probability and Statistics*. Englewood Cliffs, NJ: Prentice-Hall, 1990.

[12] J. G. Proakis, *Digital Communications*, 3rd ed. New York: McGraw-Hill, 1995.

[13] R. F. Harrington, *Field Computation by Moment Methods*. New York: IEEE Press, 1968.

[14] M. A. Richards, "SEM representation of the early and late time fields scattered from wire targets," *IEEE Trans. Antennas Propagat.*, vol. AP-42, pp. 564–566, Apr. 1994.

[15] J. E. Mooney, Z. Ding, and L. S. Riggs, "Robust target identification in white Gaussian noise for ultra wide-band radar systems," *IEEE Trans. Antennas Propagat.*, vol. 46, pp. 1817–1823, Dec. 1998.

Jon E. Mooney (S'94–M'98) was born in Montgomery, AL, on July 2, 1970. He received the B.E.E. (*summa cum laude*), M.S., and Ph.D. degrees in electrical engineering from Auburn University, Auburn, AL, in 1993, 1996, and 1998, respectively.

From 1993 to 1996, he was a U.S. Air Force Laboratory Graduate Fellow. He is currently a Senior Systems Engineer at Raytheon Systems, Company, Dallas, TX. His research interests include computational electromagnetics as well as statistical signal processing with application to radar target identification.

Dr. Mooney is a member of Eta Kappa Nu, Tau Beta Pi, and Phi Kappa Phi.

Zhi Ding (S'88–M'90–SM'95) received the Ph.D. degree from the School of Electrical Engineering, Cornell University, Ithaca, NY, in August 1990.

From 1990 to 1998, he was a faculty member in the Department of Electrical Engineering, Auburn University, Auburn, AL, first as an Assistant Professor and later as an Associate Professor. He has held visiting positions at the Australian National University, the Hong Kong University of Science and Technology, the NASA Lewis Research Center, and the USAF Wright Laboratory. He is currently an Associate Professor in the Department of Electrical and Computer Engineering at the University of Iowa, Iowa City. His research covers a number of issues involving statistical signal processing that include communications system design, signal detection and classification, as well as blind multiple-signal separation.

Dr. Ding has been an associate editor of the IEEE TRANSACTIONS ON SIGNAL PROCESSING. He currently serves as a member of the IEEE Signal Processing for Communications Technical Committee.

Lloyd S. Riggs (SM'98) received the Ph.D. degree from Auburn University, Auburn, AL, in 1985.

Prior to receiving the Ph.D. degree, he spent three years as an Antenna Design Engineer with the Electronics Systems Division at Harris Corporation, Palm Bay, FL. While at Harris, he was involved in the design of frequency selective surfaces (FSS) with application to dual and multiband radomes and satellite antennas. He was also involved in the synthesis of space-borne reflector antenna configurations for military communication and commercial direct broadcast contoured beam applications. Since the end of 1983, he has worked in the Electrical Engineering Department at Auburn University, AL. In this capacity he has been the Principal Investigator on a variety of research projects with both industry and government. He has worked with the Antenna Group of Raytheon Systems Corporation (formerly Texas Instruments), McKinney, TX, using the transmission-line matrix method (TLM) of numerical analysis to develop algorithms useful in the analysis and design of microwave devices. He has also worked with the Jet Propulsion Laboratory (JPL), Pasadena, CA, using TLM to design a stepped-septum polarizer for the Cassini (Saturn Orbiter/Titan Probe) mission. He consults with the U.S. Army Missile Command, Huntsville, AL, and in this capacity has been involved in research to identify targets based on their high-range resolution radar (HRR) signatures. He is interested in electromagnetic-based sensors [ground penetrating radar (GPR)] for the detection and identification of buried anomalies (mines). He is currently working with the U.S. Army's Night Vision Laboratory, Belvoir, VA, using the low-frequency quasi-magnetostatic response of finitely conducting objects to reduce false alarms in metal detectors. He is presently serving as the Major Professor for three master's and one Ph.D. candidate. Since 1983 he has served as the Major Professor for over 18 graduate students. He has published more than 20 refereed journal articles and 30 conference papers.

Dr. Riggs received the Best Paper of the Year Award (with T. H. Shumpert and J. Lindsey) in the IEEE TRANSACTIONS ON ELECTROMAGNETIC COMPATIBILITY in 1990.